AGU PUBLICATIONS

JGR

Journal of Geophysical Research: Space Physics

RESEARCH ARTICLE
10.1002/2017JA024146

Key Points:
- The zonal distribution of scintillation is related to the westward tilting of plasma bubbles
- There are equinoctial asymmetries in the zonal distribution of scintillation, the westward tilting of plasma bubbles, the latitudinal variation of zonal plasma drift, and the latitudinal variation of zonal neutral wind
- The zonal neutral wind and the ionospheric plasma drift are coupled through the *F* region dynamo

Correspondence to:
P. Abadi,
p-abadi@isee.nagoya-u.ac.jp

Citation:
Abadi, P., Y. Otsuka, K. Shiokawa, A. Husin, H. Liu, and S. Saito (2017), Equinoctial asymmetry in the zonal distribution of scintillation as observed by GPS receivers in Indonesia, *J. Geophys. Res. Space Physics*, *122*, 8947–8958, doi:10.1002/2017JA024146.

Received 14 MAR 2017
Accepted 7 AUG 2017
Accepted article online 11 AUG 2017
Published online 24 AUG 2017

Equinoctial asymmetry in the zonal distribution of scintillation as observed by GPS receivers in Indonesia

P. Abadi[1,2], Y. Otsuka[1], K. Shiokawa[1], A. Husin[2], Huixin Liu[3], and S. Saito[4]

[1]Institute for Space-Earth Environmental Research, Nagoya University, Nagoya, Japan, [2]Space Science Center, Indonesian National Institute of Aeronautics and Space (LAPAN), Bandung, Indonesia, [3]Department of Earth and Planetary Science, Kyushu University, Fukuoka, Japan, [4]National Institute of Maritime, Port, and Aviation Technology, Electronic Navigation Research Institute, Tokyo, Japan

Abstract We investigate the azimuthal distribution of amplitude scintillation observed by Global Positioning System (GPS) ground receivers at Pontianak (0.0°S, 109.3°E; magnetic latitude: 9.8°S) and Bandung (6.9°S, 107.6°E; magnetic latitude: 16.7°S) in Indonesia in March and September from 2011 to 2015. The scintillation is found to occur more to the west than to the east in March at both stations, whereas no such zonal difference is found in September. We also analyze the zonal scintillation drift as estimated using three closely spaced single-frequency GPS receivers at Kototabang (0.2°S, 100.3°E; magnetic latitude: 9.9°S) in Indonesia during 2003–2015 and the zonal thermospheric neutral wind as measured by the CHAMP satellite at longitudes of 90°–120°E during 2001–2008. We find that the velocities of both the zonal scintillation drift and the neutral wind decrease with increasing latitudes. Interestingly, the latitudinal gradients of both the zonal scintillation drift and the neutral wind are steeper in March than in September. These steeper March gradients may be responsible for the increased westward altitudinal and latitudinal tilting of plasma bubbles in March. This equinoctial asymmetry could be responsible for the observed westward bias in scintillation in March, because the scintillation is more likely to occur when radio waves pass through longer lengths of plasma irregularities in the plasma bubbles.

1. Introduction

In equatorial and low-latitude regions, scintillation on the L band of the Global Positioning System (GPS) occurs mainly because of irregularities inside plasma bubbles, which are magnetic field-aligned plasma depletion structures in the equatorial ionosphere. These bubbles are generated after sunset via the Rayleigh-Taylor instabilities developing at the bottomside of the *F* region at the magnetic equator [*Sultan*, 1996] and grow simultaneously in altitudes and latitudes [e.g., *Mendillo and Baumgardner*, 1982]. The associated plasma density irregularities exist at various scales in the plasma bubbles [*Basu et al*., 1978]. Scintillation of radio waves passing through the ionosphere is caused by those irregularities that are on the same scale as the first Fresnel zone, which depends on the wavelength of the radio waves and the altitude of the irregularities [*Pi et al*., 1997]. In case of the GPS-L1 band (1.57542 GHz), amplitude scintillation is caused by irregularities on a scale of ~400 m at an altitude of ~300 km.

Morphological studies of plasma bubbles show that they tilt westward and drift eastward as they extend toward higher altitudes and latitudes, have east-west extensions of between 100 km and several hundred kilometers, and have a steeper plasma density gradient at their western wall than at their eastern wall [*Mendillo and Baumgardner*, 1982]. The amplitudes of the plasma density irregularities tend to be larger in the equatorial ionization anomaly (EIA) crest region, where the plasma density is high. Therefore, scintillation tends to be concentrated in the EIA [*de Paula et al*., 2003]. In addition to the EIA, the scintillation intensity tends to be higher when the radio waves propagate nearly parallel to the magnetic field lines because irregularities inside the plasma bubbles are aligned with the magnetic field lines [*Anderson and Straus*, 2005; *Abadi et al*., 2014; *Moraes et al*., 2017]. Scintillation observed by ground receivers tends to be more frequent in an azimuth direction of westward than eastward. *Abadi et al*. [2014] attributed this to the westward tilting of plasma bubbles. Indeed, they suggested that the raypaths of westward traveling radio waves could be parallel to the plasma bubble vertical structure, and therefore, such radio waves would suffer more from scintillation effect in plasma bubbles over longer distances than those traveling eastward.

From a climatological perspective, GPS scintillation associated with plasma bubbles occurs mostly between sunset and midnight [*Basu et al*., 1978] at times of the year when the sunset terminator is aligned with the geomagnetic meridian [*Abdu et al*., 1981; *Maruyama and Matuura*, 1984; *Tsunoda*, 1985] and depends on the prevailing level of solar activity [*Basu et al*., 1988]. In the Southeast Asian longitudinal sector, more scintillation occurs around the equinoxes (March–April and September–October) [*Maruyama and Matuura*, 1984; *Nishioka et al*., 2008; *Abadi et al*., 2014]. Another interesting feature of scintillation climatology is that scintillation occurs asymmetrically between the two equinoxes [*Otsuka et al*., 2006; see also *Burke et al*., 2004]. *Otsuka et al*. [2006] analyzed GPS scintillation activity from 2003 to 2004 and found more scintillation in March–April than in September–October. Although the alignment of the solar terminator with the magnetic field explains the seasonal longitudinal variation of plasma bubble occurrence [*Abdu et al*., 1981; *Tsunoda*, 1985], it cannot account by itself for this equinoctial scintillation asymmetry. *Maruyama et al*. [2009] showed that the trans-equatorial meridional wind could be responsible for equinoctially asymmetric plasma bubble generation. They showed that the trans-equatorial wind speeds around the September equinox are higher than those around the March equinox and suggested that the trans-equatorial wind might suppress plasma bubble growth. *Otsuka et al*. [2006] reported that the eastward zonal scintillation drift after sunset is faster in March–April than in September–October. They proposed this stronger eastward drift (which could be generated by the stronger zonal eastward wind around sunset driving the *F* region dynamo) as the cause of the stronger eastward electric field that favors plasma bubble generation. However, the actual cause of the equinoctial scintillation asymmetry is still under discussion.

Abadi et al. [2014] analyzed GPS scintillation data obtained at Pontianak, Indonesia, from 2009 to 2010 and found that scintillation occurred more frequently to the west of the receiver than to the east. They suggested that this zonal difference in scintillation is due to the westward tilting of plasma bubbles. However, the equinoctial asymmetry, i.e., the difference between spring and autumn equinoxes, in the zonal scintillation distribution observed by the ground receiver has not been studied yet. Here we aim to identify the cause of the different zonal scintillation distributions between the March and September equinoxes. We discuss the possibility that the latitudinal gradients of the zonal irregularity drift and the neutral wind are both responsible for the westward tilting of plasma bubbles.

2. Observations

We used ground GPS receivers at two sites to observe the scintillation activity around the EIA region in the western part of Indonesia. The ground stations were located at Pontianak (PTK; 0.0°S, 109.3°E; magnetic latitude: 9.8°S) and Bandung (BDG; 6.9°S, 107.6°E; magnetic latitude: 16.7°S). Figure 1 shows the geographic locations of the receivers used in this study. We used the S_4 index to investigate the amplitude scintillation of the L1 signal due to ionospheric irregularities inside plasma bubbles. The S_4 index is the ratio between the standard deviation of the received signal intensity and its average value over a certain period [*Kintner et al*., 2007]. The receivers at the PTK and BDG stations were GSV4004B units that recorded the carrier-to-noise ratio at the L1 frequency with a sampling rate of 50 Hz and provided values of the S_4 index at 1 min intervals. These units also provided values of the standard deviation of code-carrier divergence (sigma-CCD) parameter, which can be used to separate multipath effects from ionospheric scintillation. In this case, we used the sigma-CCD parameter to exclude the scintillation due to multipath effects that occurs frequently at low-elevation angles; in this study, we used scintillation data at elevation angles as low as 10°. We applied the technique reported by *Abadi et al*. [2014] for using the sigma-CCD parameter to exclude multipath effects from scintillation data. Note that we used the same receivers as did *Abadi et al*. [2014]. We have analyzed the scintillation data obtained at these sites each day between 1900 and 2400 LT (local time) in March and September from 2011 to 2015 with the data availability at both PTK and BDG stations.

We also investigated the latitudinal variations of the zonal scintillation drift velocities, using three closely spaced GPS single-frequency (L1) receivers (Ashtech G12 units) that recorded the carrier-to-noise ratio at the L1 frequency with a sampling rate of 20 Hz. They are located at relative distances on the order of 100 m. They were installed at the station at Kototabang (KTB; 0.2°S, 100.3°E; magnetic latitude: 9.9°S) in Indonesia, which is located at the same latitude as the PTK station but a further 9°W in longitude. The inset in Figure 1 shows the configuration of these three GPS receivers; two were positioned east-west to be aligned geographically and magnetically with the zonal direction and the third was positioned to the south (for

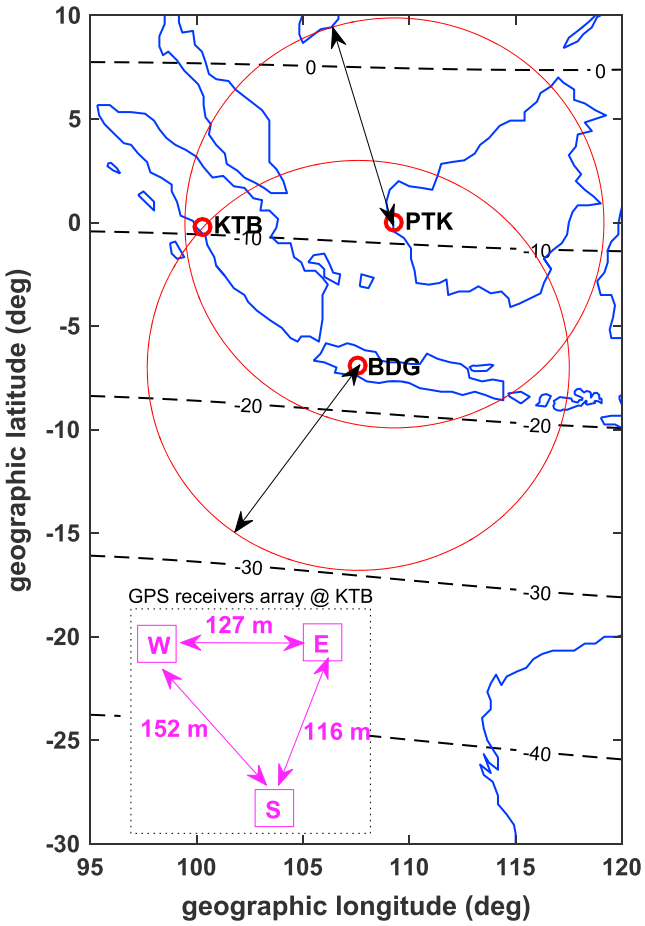

Figure 1. Geographic locations of the GPS receivers used in this study. The black dashed lines show magnetic latitudes at an altitude of 300 km. The red circles show the fields of view at an altitude of 300 km for the GPS receivers at the BDG and PTK stations.

details, see *Otsuka et al.* [2006]). We used the method of *Otsuka et al.* [2006] for estimating scintillation drift velocity. The time lags (τ) of the perturbed L1-signal intensities for three receiver pairs were calculated at 1 min intervals by applying cross correlation to the time series of the received signal intensities for 1 min. The apparent drift velocity (v) of the irregularity causing the L1 scintillation was then obtained from d/τ, where d is the distance between the two subionospheric points of the receivers at an altitude of 300 km. Note that the v consists of the velocity of irregularity drift and satellite motion. The irregularity drift velocity relative to the ground can be obtained by subtracting the satellite velocity from the v. The latitudinal variation in scintillation drift velocity was investigated by analyzing nighttime data obtained between 2000 and 2400 LT during March and September for the 12 years from 2003 to 2015. We used only scintillation drift velocities obtained at satellite elevation angles higher than 30°, which covers magnetic latitudes from −6° to −15°.

We also analyzed the zonal neutral wind by using in situ measurements of atmospheric drag taken by the CHAMP satellite, which orbits at an altitude of ~400 km with an inclination of 87.3°; this measures neutral wind velocity using an onboard accelerometer [*Reigber et al.*, 2002; *Liu et al.*, 2006; *Sutton et al.*, 2007]. In principle, the zonal neutral wind can be discerned by subtracting the velocity of the satellite motion from the total cross-track wind derived from the total acceleration measured using the accelerometer. In this study, we used the same CHAMP zonal-wind velocity data (with a 10 s time resolution) as did *Liu et al.* [2006]. They used the CHAMP satellite to study the zonal wind in detail and reported several important findings related to the climatology of the global equatorial wind. This wind is influenced considerably by the solar flux both during the day and night. However, the wind is affected more by geomagnetic activity at night than it is during the day. Seasonally, the wind tends to be weaker around the June solstice, regardless of solar flux and geomagnetic activities. Diurnally, an eastward wind occurs between 1200–0600 MLT (magnetic local time) and 1200–0300/0400 MLT for high and low $F_{10.7}$, respectively; outside those MLT periods, the wind blows westward. *Liu et al.* [2009] showed that the eastward wind after sunset maximizes at the dip equator, with winds decreasing away from the equator. Here we investigate the latitudinal variation of the zonal thermospheric wind at longitudes of 90°E–120°E between 1900 and 2300 LT during March and September from 2001 to 2008.

3. Results

In order to investigate the scintillation rates in different directions, we divided both the azimuth and elevation angles between satellite and receiver into 10° bins. We calculated the ratio between the number of scintillations and the number of observation epochs in a 3 × 3 matrix of bins and equated this ratio

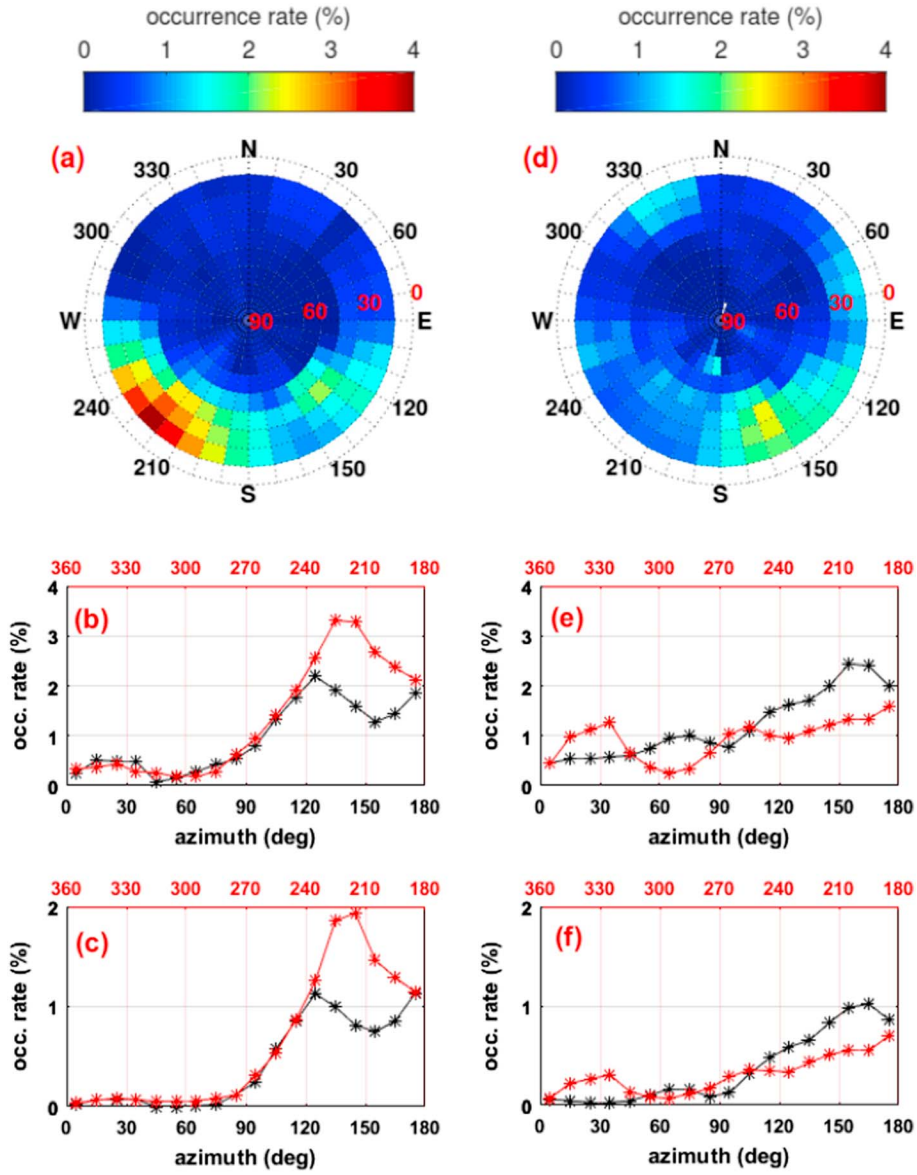

Figure 2. Distributions of scintillation rates observed at the PTK station during (a–c) March and (d–f) September. Figures 2a and 2d show the scintillation rates as sky plots, whereas Figures 2b and 2e and 2c and 2f as functions of azimuth angle when S_4 index $\geq$0.2 and S_4 index $\geq$0.5 are counted, respectively. The black and red curves in Figures 2b and 2e and 2c and 2f indicate the azimuthal dependences of eastward (0°–180° in azimuth) and westward (180°–360° in azimuth) scintillation, respectively.

with the occurrence rate at the center bin of the matrix. In this study, we used the LT at the ionospheric pierce point (IPP) at an altitude of 300 km for each satellite epoch. Only the scintillations with S_4 index $\geq$0.2 are counted in the calculation of occurrence rate. The scintillation intensity below this level is considered as noise.

Figure 2 shows the directional distributions of scintillation at PTK station during both March (Figures 2a–2c) and September (Figures 2d–2f). The azimuth is measured clockwise from due north. In Figures 2a and 2d, the panels show the scintillation occurrence rates as sky plots in which the radio wave directions from satellite to receiver are shown, and Figures 2b and 2e and 2c and 2f show the azimuthal dependencies of the scintillation rates for S_4 index larger than 0.2 and 0.5, respectively. We see a high scintillation rate across the southern sky for PTK station during both March and September, but interestingly, there is a clear difference in the March zonal scintillation distribution compared with the September one. The following points can be noted in

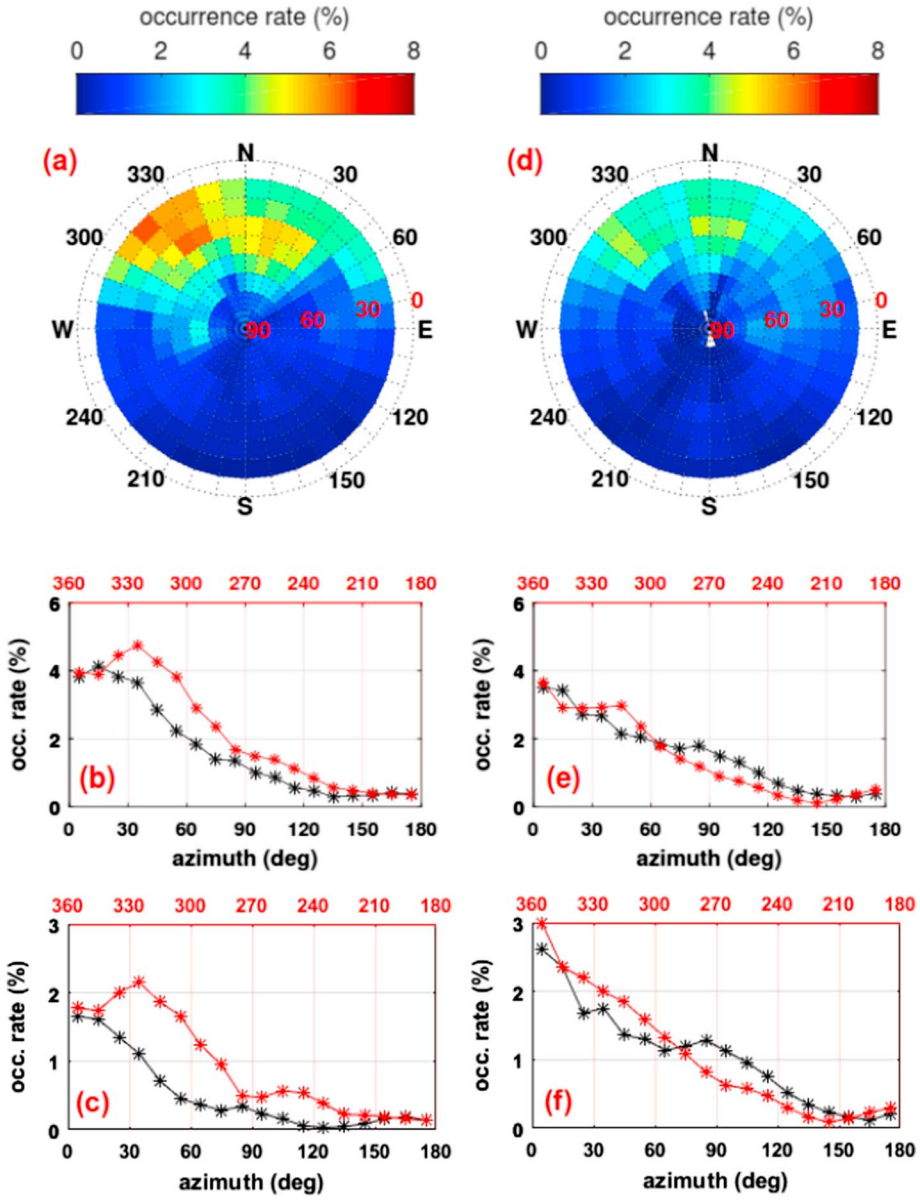

Figure 3. As for Figure 2 but at Bandung (BDG) station.

Figure 2: the westward scintillation rate is notably higher than the eastward one (Figure 2a); there is a clear tendency for more scintillation in March in the southwest (azimuth angles of 180°–240°) than in the southeast (azimuth angles of 120°–180°) (Figure 2b); this clear tendency is still consistent even though we increase scintillation intensity ($S_4 \geq 0.5$) in the occurrence rate calculation (Figure 2c); there tends to be more scintillation in the southeast in September (Figure 2d); scintillation tends to be more prominent at azimuth angles of 120°–180° (Figure 2e), and this zonal difference in scintillation in September is found to be opposite to that in March; the zonal difference in scintillation in September tends to be clearer for scintillation intensity larger than 0.5 (Figure 2f). Another feature seen in Figure 2 is that the zonal difference depends predominantly on scintillation at low-elevation angles in both March and September.

Figure 3 is as Figure 2 but for the BDG station, where scintillation occurs mostly in the northern sky during both March and September. The difference between the eastward and westward scintillation distributions is seen most clearly in March. As shown in Figures 3a–3c, scintillation in March occurs more in the northwest than in the northeast, whereas Figures 3d–3f shows scintillation in September being comparable at both

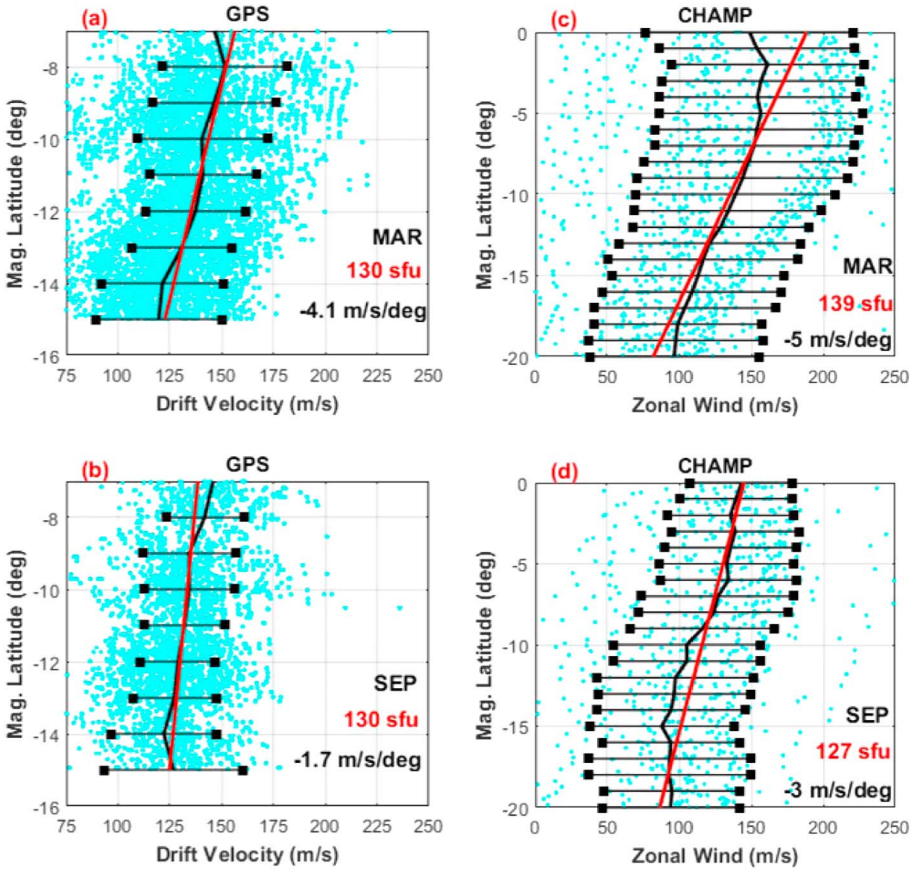

Figure 4. Latitudinal variations of zonal scintillation drift velocity during (a) March and (b) September estimated from three closely spaced GPS receivers at the KTB station. Latitudinal variations of zonal neutral wind measured using CHAMP satellite during (c) March and (d) September.

directions. As at the PTK station, the zonal difference in scintillation in BDG station is seen more clearly at lower elevation angles.

The most interesting aspect of the scintillation observations at the PTK (Figure 2) and BDG (Figure 3) stations (which are separated by 6° in latitude) is that westward scintillation is clearly more pronounced than eastward scintillation in March, whereas no such zonal difference—higher scintillation occurrence in the west compared with the occurrence in the east— is discernible in September.

Next, we show observational results for the latitudinal variations of the velocities of the zonal scintillation drifts and neutral winds. Figure 4 shows the latitudinal variations of scintillation drift velocities measured using the three closely spaced receivers at KTB station (Figures 4a and 4b) and the latitudinal variations of zonal wind velocity measured using the CHAMP satellite (Figures 4c and 4d). The velocities of zonal scintillation drifts and neutral winds are classified into two data sets, namely, in March and in September. Each dot in Figures 4a and 4b and Figures 4c and 4d indicates a scintillation drift and neutral wind velocity measured in 1 min and in 10 s, respectively. The black curve in each panel indicates the average velocity over 1° of magnetic latitudes, and the bars indicate its standard deviations. The red line in each panel shows the linear fits to the 1 min data and the 10 s data from −8° to −15° and from −5° to −20° in magnetic latitudes for the velocities of scintillation drifts and neutral winds, respectively. The black and red numbers show the latitudinal gradients obtained from the linear fit of velocity (red line) and the average value of daily $F_{10.7}$, respectively. As shown in Figures 4a and 4b, the average zonal scintillation drift velocity decreases with magnetic latitude in both March and September. Our results are consistent with those of *Kil et al.* [2002], who showed that the zonal velocity of scintillation drift decreases from the magnetic equator to the EIA region in the Brazilian longitudinal sector, and agree with the results of *Sobral and Abdu* [1991] on latitudinal variation in plasma bubble drift (measured optically) in the Brazilian sector.

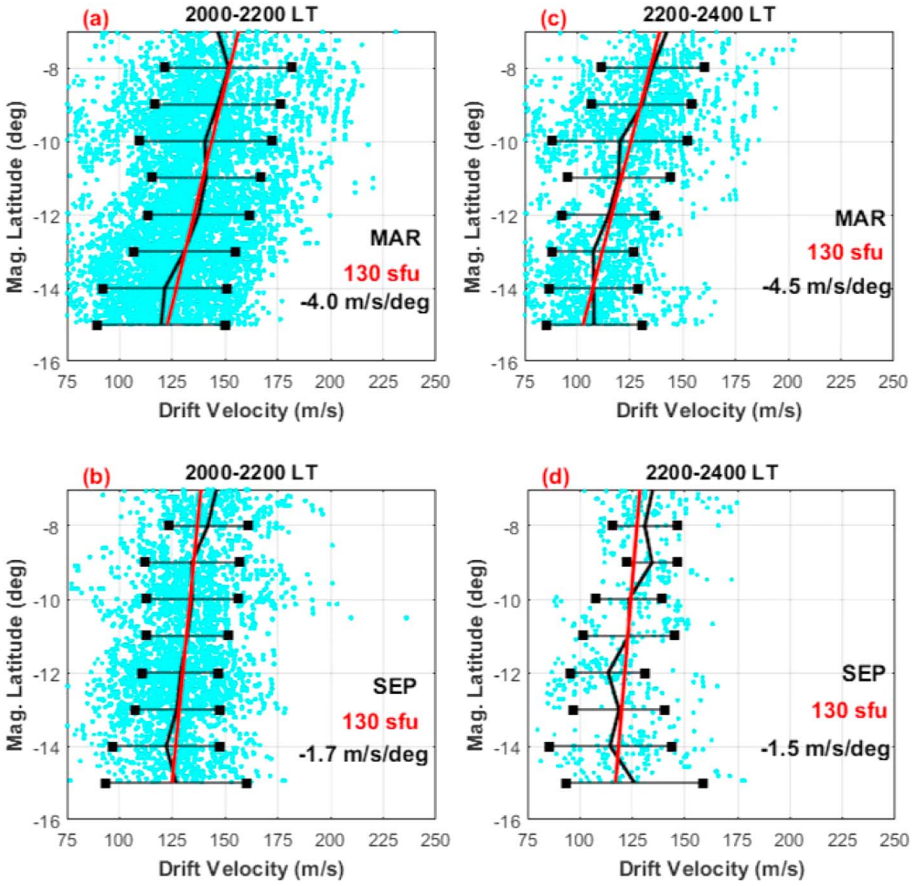

Figure 5. Latitudinal profiles of scintillation drift velocity for 2000–2200 LT during (a) March and (b) September and for 2200–2400 LT during (c) March and (d) September.

We now emphasize the difference between the latitudinal gradients of zonal scintillation drift in March and September, which are −4.1 m/s/deg and −1.7 m/s/deg, respectively. Comparing the latitudinal gradients of zonal scintillation drift in those two equinoctial months, we find that the one in March is approximately twice as steep as the one in September. The average daily $F_{10.7}$ index is the same in both March and September (roughly 130 sfu (solar flux unit)). Thus, we suggest that the current results are not affected by mixing those solar activity dependencies.

The accuracy of drift velocity measurement is estimated to be 4 m/s on the basis of a signal intensity sampling rate of 20 Hz, a receiver separation on the order of 100 m, and a typical drift velocity of 100 m/s [see *Otsuka et al.*, 2006]. Therefore, the wide scatter observed in the measured drift velocities cannot be attributed to measurement error alone but also to the effects of (i) fluctuations in drift velocity during the initial phase of plasma bubble generation, (ii) local time variations, (iii) magnetic activity, and (iv) day-to-day variability of drift velocity. We discuss these various possibilities below.

In this study, we used drift-velocity data from only 2000 to 2400 LT during both March and September because those from 1800 to 2000 LT were found to fluctuate excessively. This was probably because the latter local time period corresponds to the initial phase of generation for both plasma bubbles and plasma density irregularities. Hence, we excluded the drift data from this local time period to minimize the velocity fluctuations. The drift velocity also experienced local time variations, it being highest after sunset and then decreasing with time. We have analyzed the latitudinal variation of drift velocity in the same way as shown in Figures 4a and 4b but classified into two groups based on local time period, namely, 2000–2200 LT and 2200–2400 LT. Figure 5 shows the latitudinal variations of drift velocity for the two local time groups during both March and September. As shown in Figure 5, the latitudinal profile of drift velocity is steeper in March than it is in September for both groups. The latitudinal gradient of drift velocity was maintained from 2000 to

2400 LT. As for the effect of magnetic activity, we used only drift velocity data that was obtained during magnetically quiet periods, which is defined as a condition that the maximum *Kp* index during 0600–1200 UT (around 1300–1900 LT in longitude of ~107°E) is less than 3, because *Carter et al*. [2014] have shown that the modeled zonal wind at the equator varied linearly with *Kp* from hours earlier (see their Figure 3c). During the night, the plasma motion in the equatorial region and the low-latitude *F* region is caused by the neutral wind via the *F* region dynamo. *Liu et al*. [2006] showed that the nighttime thermospheric wind has a high day-to-day variability, which means that the same is true for the nighttime drift velocity; this may be the main cause of the scatter in our drift-velocity data.

Figures 4c and 4d show the latitudinal shear of the zonal neutral wind velocity deduced from in situ measurements from the CHAMP satellite. Because the zonal neutral wind (particularly at night) is influenced by magnetic activity [*Liu et al*., 2006], we used only zonal wind data obtained during magnetically quiet periods. We note that the period of the zonal wind data used in this study is different from that of the scintillation observations. However, the average daily $F_{10.7}$ value for the days used for wind data analysis is not significantly different from that for the days used for scintillation drift analysis. As shown in Figures 4c and 4d, the average daily $F_{10.7}$ values for wind data sets of March and September are 139 and 127 sfu, respectively. We also note that the latitudinal variation of zonal neutral wind velocity is highly scattered. We found that the zonal wind velocity data from CHAMP for both March and September are not equally distributed in local time and solar activity level. In the March data set, the majority of data with $F_{10.7} \geq 150$ are from 1800 to 2000 LT and the majority with $F_{10.7} < 150$ are from 2100 to 2400 LT, whereas for the September data the equivalent correspondences are ($F_{10.7} \geq 150$: 2200–2400 LT) and ($F_{10.7} < 150$: 1800–2300 LT). Hence, the wind velocity shows a local time variation, with the velocity being higher after sunset and lower around midnight. In addition, the eastward wind velocity shows a strong positive correlation with solar activity [*Liu et al*., 2006]. To deal with these local time effects, we used data points from 1900 to 2300 LT in order to minimize the statistical errors associated with local time and solar activity in the calculation of average latitudinal wind velocity.

As with the latitudinal variation of scintillation drift velocity, we also found that the latitudinal variation of zonal wind velocity showed a negative gradient during both March and September. In Figures 4c and 4d, we see that the zonal wind velocity is largest at the magnetic equator and decreases with latitude. This feature is the so-called equatorial thermosphere jet reported in *Liu et al*. [2009] using the CHAMP observations and is consistent with DE-2 observations shown in *Raghavarao et al*. [1991] and the GOCE observations shown in *Liu et al*. [2016]. Coincidently, we found a steeper latitudinal gradient of zonal wind velocity in March than in September: −5.0 m/s/deg and −3.0 m/s/deg, respectively. We note a difference of roughly 35 m/s in wind velocity at a magnetic latitude of −5° between March and September, although this is within one standard deviation. The total systematic error in the wind measurements from the CHAMP satellite is 15 m/s, increasing to 22 m/s near the terminator time [see *Liu et al*., 2006, Appendix A]; hence, we excluded wind data near the terminator time. Therefore, a difference of roughly 35 m/s in wind velocity could be due to the different natural conditions in March and September, rather than being from measurement error. This is also consistent with a statistical analysis of CHAMP wind during 2000–2010, showing larger wind speed around March equinox than around September equinox [*Liu et al*., 2016, Figure 6]. As stated earlier, we attribute the high degree of scatter in the wind analysis data to the high daily variation in nighttime wind velocity.

4. Discussion

As shown in Figures 2 and 3, scintillation is more pronounced to the south at PTK and to the north at BDG. With PTK and BDG being located at magnetic latitudes of −9.8° and −16.7°, respectively, these findings can be attributed to the average location of the EIA crest over the Indonesian longitudinal sector, as reported by *Abadi et al*. [2014]. It is well known that the strength of amplitude scintillation is proportional to the amplitude of the plasma density perturbations [*Basu et al*., 1976; *Aarons*, 1977; *Yeh and Liu*, 1982]. Therefore, the strongest amplitude scintillation tends to occur in the region with the highest background density. The plasma density is relatively high in the EIA crest, so amplitude scintillation is stronger around the EIA region and occurs there more frequently [*de Paula et al*., 2003]. Hence, the more pronounced southward (northward) scintillation at PTK (BDG) is because the EIA crest is located between PTK and BDG.

We also note that the scintillation rates at both PTK and BDG are higher at lower elevation angles during both March and September. Radio waves arriving at lower elevation angles are more likely to have suffered from

multipath effects in the vicinity of the receiver. However, multipaths can occur at fixed directions during any season if the environment around the receiver is invariant. The current observational results show a difference between the azimuthal distributions of scintillation rate in March and September. Consequently, the scintillation observed at both PTK and BDG could not have been caused by multipath effects, but must instead have been caused by ionospheric scintillations due to ionospheric irregularities.

As part of our overall goal, we focus on this difference between the March and September zonal scintillation distributions. Our findings show clearly that the higher westward scintillation (compared with the eastward scintillation) during March pertains to both stations used in this study, whereas the September zonal scintillation difference is not the same for both stations. We will consider three factors that may affect the zonal scintillation distribution, namely, the east-west density gradient, the longitudinal variability of plasma bubble occurrence, and the westward tilting of plasma bubbles. Of these factors, we suggest that the westward tilting of plasma bubbles is the main cause of the zonal scintillation difference observed by the ground receivers, as suggested also by *Abadi et al*. [2014]. Furthermore, this suggestion implies that plasma bubbles are tilted further westward in March than they are in September. Next, we discuss possible reasons for highlighting westward plasma bubble tilting as the dominant factor in the zonal scintillation distribution.

As mentioned above, the background plasma density can affect scintillation intensity. Therefore, we examine the longitudinal plasma density variations as a possible cause of zonal scintillation distribution detected by the ground receivers. We consider that local time differences may cause an east-west plasma density gradient. At the sunset terminator, the plasma density to the west of a receiver tends to be higher than that to the east because plasma density decreases with local time, and this east-west density gradient may contribute to higher scintillation to the west of the receiver. In order to avoid these local time effects, as stated earlier, we used the local time at the IPP at which scintillation was observed, thereby eliminating any east/west bias from our results. Furthermore, for an east-west plasma density gradient related to local time difference to be the main factor in the zonal scintillation distribution, the latter would have to be the same in both March and September. However, our observations show that the asymmetric east-west scintillation distribution, in particular higher westward scintillation compared with one in eastward, pertains only to March. Thus, the east-west plasma density gradient due to local time differences cannot be a contributing factor to the zonal scintillation distribution.

Alternatively, the zonal scintillation distributions observed at PTK and BDG could be attributed in principle to longitudinal variations in plasma bubble occurrence. By using multibeam steering radars at Kototabang in Indonesia (0.2°S, 100.3°E) and Sanya in China (18.4°N, 109.6°E), *Li et al*. [2016] found that occurrence rates of plasma bubble at two sites are comparable, although the generation rate of plasma bubble over Kototabang is almost twice higher than those over Sanya. They argued that the two occurrence rates were in fact comparable because plasma bubbles move eastward from Kototabang to Sanya over a distance of roughly 1,000 km. Consequently, longitudinal variations in plasma bubble occurrence do not contribute to the zonal scintillation distribution.

In addition to higher plasma density leading to stronger irregularities, the intensity of scintillation on GPS signals is affected also by the radio wave path lengths through the irregularities. In the case of westward tilted plasma bubbles, the raypaths of radio waves from a satellite in the western sky (compared with one in the eastern sky) would be more parallel to the plasma bubble structures. Thus, radio waves from the west are likely to propagate through more plasma bubble irregularities than those from the east, and the possibility of enhanced scintillation intensity (usually expressed in the literature as the S_4 index) due to longer propagation path along the westward-tilted vertical bubble irregularity structure is understandable for the case of observations in the western azimuth. On the other hand, less intense scintillation should be present for observations in eastern azimuth. Hence, our observations in March shown in Figures 2 and 3 support the conclusion that westward plasma bubble tilting can be the main cause of the higher westward scintillation occurrence.

In addition, based on Figures 2 and 3, we reported that this east-west scintillation asymmetry was more pronounced in March compared with September as observed from all stations used in this study. Hence, we turn now to a possible cause of this observation. We speculate that the westward plasma bubble tilting is more pronounced around the March equinox than it is around the September equinox. In fact, the scintillation distribution, looking from PTK station, in September shows enhanced occurrence predominantly in the

south-eastern azimuth region, which may not fit with the westward tilting of the bubble structure. In order to test this hypothesis, we investigate the latitudinal variations in the velocities of the zonal scintillation drift and neutral wind and discuss their differences between March and September.

A latitudinal variation in drift velocity corresponds to a vertical variation in drift velocity on the vertical plane at the equator [*Kil et al*., 2002], because an electric field is mapped without attenuation along the magnetic field lines between the northern and southern hemispheres [*Saito et al*., 1995]. We assume that the average scintillation drift corresponds to the background plasma drift. Thus, based on Figures 4a and 4b, our findings in relation to the negative gradient in the latitudinal variation of scintillation drift indicate a negative gradient in the altitudinal variation of the background plasma drift on the equatorial plane. Hence, the altitudinal/latitudinal variation of eastward background plasma drift could be responsible for the westward tilting of plasma bubbles [*Woodman and La Hoz*, 1976; *Zalesak et al*., 1982; *Kil et al*., 2009]. The zonal background plasma drift is caused by the zonal neutral wind via the *F* region dynamo process. Our observations shown in Figures 4c and 4d reveal that the latitudinal gradient in wind velocity is steeper in March than in September. This result supports the hypothesis that plasma bubbles are tilted westward more in March than in September and suggests that this equinoctial asymmetry of westward plasma bubble tilting is due to the equinoctial asymmetry in the latitudinal gradient of the zonal neutral winds.

We found that the magnitude of the average zonal scintillation drift is not comparable with that of the average neutral wind velocity. It should be noted that the velocity discussed in this study is not that of background plasma drift but rather the drift velocity of the plasma bubble irregularities that cause the GPS-L1 scintillation. Many previous studies have reported that irregularities inside a plasma bubble do not move according to the background plasma drift velocity [e.g., *Huang et al*., 2010; *England and Immel*, 2012; *Chapagain et al*., 2013; *Kil et al*., 2014]. In fact, this study measured the zonal scintillation drift and neutral wind at altitudes of ~300 km and ~400 km, respectively. Since the zonal wind is the driver for the zonal plasma drift through *F* region dynamo, this difference between the two zonal velocities should imply a negative height gradient; that is, the velocity decreasing from 300 km to 400 km (at all latitudes of the observations) should directly contribute to the westward tilt of the bubble vertical structure. However, in the present study, we do not discuss this discrepancy between scintillation drift and background plasma motion in detail. Instead, we focus on the differences in the latitudinal gradients of zonal scintillation drift and wind velocity between March and September. There appears to be a correspondence between the equinoctial difference in the latitudinal gradient of scintillation drift (plasma condition) and that in the latitudinal gradient of zonal wind velocity (neutral condition). Both latitudinal variations show steeper gradients in March than in September. Thus, we suggest that the equinoctial asymmetries in these latitudinal variations of plasma and neutral could be responsible for the westward bias in scintillation occurrence being observed more in March than in September.

The equinoctial asymmetries in neutral wind and thermospheric composition could be responsible for the equinoctial asymmetry in the ionosphere [*Balan et al*., 1998]. This result is consistent with our findings that the equinoctial asymmetry in the latitudinal profile of the zonal plasma drift can be attributed to that in the latitudinal profile of the thermospheric wind. By using ROCSAT-1 satellite observations from 1999 to 2004, *Ren et al*. [2011] showed clearly that the maximum electric field at the sunset terminator—the so-called pre-reversal enhancement (PRE)—in the equatorial region at longitudes of 150°–320° is higher at the March equinox than at the September equinox. Such asymmetry has been observed over South America from ground-based measurement as well [see, for example, *Abdu et al*., 2004, Figure 9]. They also considered the equinoctial asymmetry in PRE to be caused by the equinoctial asymmetry in thermospheric wind via the *F* region dynamo process.

Abdu et al. [2009] described the important roles of gravity wave (GW) on the plasma bubble generation, namely: GW directly provide a seed or an initiation for the bubble generation through modulating *F* region altitude and/or density perturbations; GW could also modulate the background eastward thermospheric wind that can influence PRE strength which is an important factor for the bubble generation. Therefore, we consider that the equinoctial asymmetry in the existence of GW in the ionosphere, though it has not been reported yet by previous studies, could cause equinoctial asymmetry in the plasma bubble occurrence. In relation to the focus of this study, we may consider another aspect for the role of GW on plasma bubble evolution; that is, the eastward thermospheric wind induced by GW may also affect the altitudinal/latitudinal

structure of plasma bubble. Some of the upward propagating GWs generated in the lower atmosphere reach the thermosphere and deposit momentum into the background atmosphere upon breaking. In addition, some secondary GWs generated around/below the mesopause region reach the thermosphere [*Vadas and Nicolls*, 2012]. These waves also break in the thermosphere and deposit momentum into the background atmosphere, causing acceleration/deceleration of the thermospheric wind [*Vadas and Liu*, 2011]. *Alexander et al*. [2008] used the Equatorial Atmosphere Radar at Kototabang, Indonesia, to investigate the 5 year seasonal variation of upward flux of the zonal momentum transferred by GWs below an altitude of 12 km and found that the zonal momentum of GWs with periods of less than 24 h was eastward for all year long (see their Figure 11b). In that figure, the eastward momentum flux can be seen to be larger in March than in September. This indicates an equinoctial difference in the GW momentum flux in the lower atmosphere over Western Indonesia, which is the same region covered in our study. We thus consider it possible that this equinoctial asymmetry in the GW momentum deposits in the thermosphere could be responsible for the equinoctial asymmetry in the nighttime thermospheric neutral wind, and consequently in the equinoctial asymmetry in the westward tilting of plasma bubble. In order to confirm this effect, we need to investigate further the extent to which such GWs propagate into the thermosphere and to estimate the amounts of momentum that they deposit there.

5. Conclusions

We have analyzed the S_4 index of amplitude scintillation as observed by GPS ground receivers at Pontianak and Bandung in Indonesia during March and September from 2011 to 2015. We did this analysis in order to study the equinoctial asymmetry in the zonal distributions of scintillation occurrence. Our most important finding is that scintillation in March occurs more in the western azimuth than in the eastern azimuth as observed from all stations, whereas no such zonal scintillation difference is discernible in September. Because a higher westward scintillation is indicative of a westward tilting of plasma bubbles, our observational results suggest that plasma bubbles are tilted westward in altitude/latitude more in March than they are in September. In order to check this hypothesis, we investigated latitudinal variations in zonal scintillation drifts as estimated using three closely spaced GPS receivers and CHAMP satellite measurements of the neutral thermospheric wind. We found that the velocities of both the scintillation drift and the neutral wind decreased with increasing magnetic latitudes, and the latitudinal gradients of both scintillation drift and neutral wind were steeper in March than in September. These observations support the idea that plasma bubbles are tilted westward more in March than in September. Consequently, we conclude that this further westward plasma bubble tilting in March could be responsible for the observed higher westward scintillation as compared with the eastward scintillation. The equinoctial asymmetry in the thermospheric winds could play an important role in the equinoctial asymmetry in the occurrence of ionospheric irregularities.

Acknowledgments

This work is supported by the Project for Solar-Terrestrial Environment Prediction (PSTEP, JP 15H05815) that is funded by a Grant-in-Aid for Scientific Research on Innovative Areas from MEXT/Japan. This work is also supported by the Japan Society for the Promotion of Science (JSPS) Core-to-Core Program, B. Asia-Africa Science Platforms. P.A. would like to thank the Ministry of Research, Technology and Higher Education of the Republic of Indonesia (RISTEKDIKTI) for supporting his PhD course at Nagoya University. He would also like to thank Rezy Pradipta of ISR, Boston College, for helpful discussions during a 2 week visit to ISR that was supported by PSTEP through an internship program for students and young scientists. H.L. acknowledges support by JSPS KAKENHI grants 15K05301, 15H02135, and 15H05815. The scintillation data from the PTK and BDG stations that was used in this study can be obtained on request from A.H. (asnawi@lapan.go.id). The scintillation drift data from the KTB station can be obtained on request from Y.O. (otsuka@isee.nagoya-u.ac.jp). The $F_{10.7}$ and *Kp* index data used in this study were obtained from the OMNIWeb website, https://omniweb.gsfc.nasa.gov/form/dx1.html.

References

Aarons, J. (1977), Equatorial scintillations: a review, *IEEE Trans. Antennas Propag.*, *AP-25*(5), 729–736.

Abadi, P., S. Saito, and W. Srigutomo (2014), Low-latitude scintillation occurrences around the equatorial anomaly crest over Indonesia, *Ann. Geophys.*, *32*, 7–17, doi:10.5194/angeo-32-7-2014.

Abdu, M. A., I. S. Batista, B. W. Reinisch, and A. J. Carrasco (2004), Equatorial *F*-layer heights, evening prereversal electric field, and night *E*-layer density in the American sector: IRI validation with observations, *Adv. Space Res.*, *34*(9), 1953–1965, doi:10.1016/j.asr.2004.04.011.

Abdu, M. A., E. Alam Kherani, I. S. Batista, E. R. de Paula, D. C. Fritts, and J. H. A. Sobral (2009), Gravity wave initiation of equatorial spread *F*/plasma bubble irregularities based on observational data from the SpreadFEx campaign, *Ann. Geophys.*, *27*, 2607–2622, doi:10.5194/angeo-27-2607-2009.

Abdu, M. A., J. A. Bittencourt, and I. S. Batista (1981), Magnetic declination control of the equatorial F region dynamo electric field development and spread F, *J. Geophys. Res.*, *86*(A13), 11,443–11,446, doi:10.1029/JA086iA13p11443.

Alexander, S. P., T. Tsuda, Y. Shibagaki, and T. Kozu (2008), Seasonal gravity wave activity observed with the Equatorial Atmosphere Radar and its relation to rainfall information from the Tropical Rainfall Measuring Mission, *J. Geophys. Res.*, *113*, D02104, doi:10.1029/2007JD008777.

Anderson, P. C., and P. R. Straus (2005), Magnetic field orientation control of GPS occultation observations of equatorial scintillation, *Geophys. Res. Lett.*, *32*, L21107, doi:10.1029/2005GL023781.

Balan, N., Y. Otsuka, G. J. Bailey, and S. Fukao (1998), Equinoctial asymmetries in the ionosphere and thermosphere observed by the MU radar, *J. Geophys. Res.*, *103*(A5), 9481–9495, doi:10.1029/97JA03137.

Basu, S., E. MacKenzie, and S. Basu (1988), Ionospheric constraints on VHF/UHF communications links during solar maximum and minimum periods, *Radio Sci.*, *23*(3), 363–378, doi:10.1029/RS023i003p00363.

Basu, S., S. Basu, and B. K. Khan (1976), Model of equatorial scintillations from in-situ measurements, *Radio Sci.*, *11*(10), 821–832, doi:10.1029/RS011i010p00821.

Basu, S., S. Basu, J. Aarons, J. P. McClure, and M. D. Cousins (1978), On the coexistence of kilometer- and meter-scale irregularities in the nighttime equatorial *F* region, *J. Geophys. Res.*, *83*(A9), 4219–4226, doi:10.1029/JA083iA09p04219.

Burke, W. J., C. Y. Huang, L. C. Gentile, and L. Bauer (2004), Seasonal-longitudinal variability of equatorial plasma bubbles, *Ann. Geophys.*, *22*, 3089–3098, doi:10.5194/angeo-22-3089-2004.

Carter, B. A., et al. (2014), Geomagnetic control of equatorial plasma bubble activity modeled by the TIEGCM with *Kp*, *Geophys. Res. Lett.*, *41*, 5331–5339, doi:10.1002/2014GL060953.

Chapagain, N. P., D. J. Fisher, J. W. Meriwether, J. L. Chau, and J. J. Makela (2013), Comparison of zonal neutral winds with equatorial plasma bubble and plasma drift velocities, *J. Geophys. Res. Space Physics*, *118*, 1802–1812, doi:10.1002/jgra.50238.

de Paula, E. R., F. S. Rodrigues, K. N. Iyer, I. J. Kantor, M. A. Abdu, P. M. Kintner, B. M. Ledvina, and H. Kil (2003), Equatorial anomaly effects on GPS scintillations in Brazil, *Adv. Space Res.*, *31*, 749–754.

England, S. L., and T. J. Immel (2012), An empirical model of the drift velocity of equatorial plasma depletions, *J. Geophys. Res.*, *117*, A12308, doi:10.1029/2012JA018091.

Huang, C.-S., O. de La Beaujardiere, R. F. Pfaff, J. M. Retterer, P. A. Roddy, D. E. Hunton, Y.-J. Su, S.-Y. Su, and F. J. Rich (2010), Zonal drift of plasma particles inside equatorial plasma bubbles and its relation to the zonal drift of the bubble structure, *J. Geophys. Res.*, *115*, A07316, doi:10.1029/2010JA015324.

Kil, H., R. A. Heelis, L. J. Paxton, and S.-J. Oh (2009), Formation of a plasma depletion shell in the equatorial ionosphere, *J. Geophys. Res.*, *114*, A11302, doi:10.1029/2009JA014369.

Kil, H., W. K. Lee, Y.-S. Kwak, Y. Zhang, L. J. Paxton, and M. Milla (2014), The zonal motion of equatorial plasma bubbles relative to the background ionosphere, *J. Geophys. Res. Space Physics*, *119*, 5943–5950, doi:10.1002/2014JA019963.

Kil, H., P. M. Kintner, E. R. de Paula, and I. J. Kantor (2002), Latitudinal variations of scintillation activity and zonal plasma drifts in South America, *Radio Sci.*, *37*(1), 1006, doi:10.1029/2001RS002468.

Kintner, P. M., B. M. Ledvina, and E. R. de Paula (2007), GPS and ionospheric scintillations, *Space Weather*, *5*, S09003, doi:10.1029/2006SW000260.

Li, G., Y. Otsuka, B. Ning, M. A. Abdu, M. Yamamoto, W. Wan, L. Liu, and P. Abadi (2016), Enhanced ionospheric plasma bubble generation in more active ITCZ, *Geophys. Res. Lett.*, *43*, 2389–2395, doi:10.1002/2016GL068145.

Liu, H., E. Doornbos, and J. Namashima (2016), Thermospheric wind observed by GOCE: Wind jets and seasonal variations, *J. Geophys. Res. Space Physics*, *121*, 1–13, doi:10.1002/2016JA022938.

Liu, H., S. Watanabe, and T. Kondo (2009), Fast thermospheric wind jet at the Earth's dip equator, *Geophys. Res. Lett.*, *36*, L08103, doi:10.1029/2009GL037377.

Liu, H., S. Watanabe, W. Kohler, V. Henize, and P. Visser (2006), Zonal winds in the equatorial upper thermosphere: Decomposing the solar flux, geomagnetic activity, and seasonal dependencies, *J. Geophys. Res.*, *111*, A07307, doi:10.1029/2005JA011415.

Maruyama, T., and N. Matuura (1984), Longitudinal variability of annual changes in activity of equatorial spread *F* and plasma bubbles, *J. Geophys. Res.*, *89*(A12), 10903–10912, doi:10.1029/JA089iA12p10903.

Maruyama, T., S. Saito, M. Kawamura, K. Nozaki, J. Krall, and J. D. Huba (2009), Equinoctial asymmetry of a low-latitude ionosphere-thermosphere system and equatorial irregularities: Evidence for meridional wind control, *Ann. Geophys.*, *27*, 2027–2034, doi:10.5194/angeo-27-2027-2009.

Mendillo, M., and J. Baumgardner (1982), Airglow characteristics of equatorial plasma depletions, *J. Geophys. Res.*, *87*(A9), 7641–7652, doi:10.1029/JA087iA09p07641.

Moraes, A. O., E. Costa, M. A. Abdu, F. S. Rodrigues, E. R. de Paula, K. Oliveira, and W. J. Perrella (2017), The variability of low-latitude ionospheric amplitude and phase scintillation detected by a triple-frequency GPS receiver, *Radio Sci.*, *52*, 439–460, doi:10.1002/2016RS006165.

Nishioka, M., A. Saito, and T. Tsugawa (2008), Occurrence characteristics of plasma bubble derived from global ground-based GPS receiver networks, *J. Geophys. Res.*, *113*, A05301, doi:10.1029/2007JA012605.

Otsuka, Y., K. Shiokawa, and T. Ogawa (2006), Equatorial ionospheric scintillations and zonal irregularity drifts observed with closely-spaced GPS receivers in Indonesia, *J. Meteorol. Soc. Jpn.*, *84A*, 343–351.

Pi, X., A. J. Mannucci, U. J. Lindqwister, and C. M. Ho (1997), Monitoring of global ionospheric irregularities using the Worldwide GPS Network, *Geophys. Res. Lett.*, *24*(18), 2283–2286, doi:10.1029/97GL02273.

Raghavarao, R., L. E. Wharton, N. W. Spencer, H. G. Mayr, and L. H. Brace (1991), An equatorial temperature and wind anomaly (ETWA), *Geophys. Res. Lett.*, *18*(7), 1944–8007, doi:10.1029/91GL01561.

Reigber, C., H. Luhr, and P. Schwintzer (2002), CHAMP mission status, *Adv. Space Res.*, *30*(2), 129–134, doi:10.1016/S0273-1177(02)00276-4.

Ren, Z., W. Wan, L. Liu, Y. Chen, and H. Le (2011), Equinoctial asymmetry of ionospheric vertical plasma drifts and its effect on *F*-region plasma density, *J. Geophys. Res.*, *116*, A02308, doi:10.1029/2010JA016081.

Saito, A., T. Iyemori, M. Sugiura, N. C. Maynard, T. L. Aggson, L. H. Brace, M. Takeda, and M. Yamamoto (1995), Conjugate occurrence of the electric field fluctuations in the nighttime midlatitude ionosphere, *J. Geophys. Res.*, *100*(A11), 21,439–21,451, doi:10.1029/95JA01505.

Sobral, J. H. A., and M. A. Abdu (1991), Solar activity effects on equatroial plasma bubble zonal velocity and its latitude gradient as measuerd by airglow scanning photometers, *J. Atmos. Terr. Phys.*, *53*(8), 729–742, doi:10.1016/0021-9169(91)90124-P.

Sultan, P. J. (1996), Linear theory and modeling of the Rayleigh-Taylor instability leading to the occurrence of equatorial spread *F*, *J. Geophys. Res.*, *101*(A12), 26875–26891, doi:10.1029/96JA00682.

Sutton, E. K., R. S. Nerem, and J. M. Forbes (2007), Density and winds in thermosphere deduced from accelerometer data, *J. Spacecr. Rockets*, *44*(6), 1210–1219, doi:10.2514/1.28641.

Tsunoda, R. T. (1985), Control of the seasonal and longitudinal occurrence of equatorial scintillations by the longitudinal gradient in integrated *E* region Pedersen conductivity, *J. Geophys. Res.*, *90*(A1), 447–456, doi:10.1029/JA090iA01p00447.

Vadas, S. L., and H.-L. Liu (2011), Neutral winds and densities at the underside of the *F* layer from primary and secondary gravity waves from deep convection, in *Aeronomy of the Earth's Atmosphere and Ionosphere*, pp. 131–139, Springer, New York.

Vadas, S. L., and M. J. Nicolls (2012), The phases and amplitudes of gravity waves propagating and dissipating in the thermosphere: Theory, *J. Geophys. Res.*, *117*, A05322, doi:10.1029/2011JA017426.

Woodman, R. F., and C. La Hoz (1976), Radar observations of *F* region equatorial irregularities, *J. Geophys. Res.*, *81*(31), 5447–5466, doi:10.1029/JA081i031p05447.

Yeh, K. C., and C. H. Liu (1982), Radio wave scintillation in the ionosphere, *Proc. IEEE*, *70*, 324–360.

Zalesak, S. T., S. L. Ossakow, and P. K. Chaturvedi (1982), Nonlinear equatorial spread *F*: The effect of neutral winds and background Pedersen conductivity, *J. Geophys. Res.*, *87*(A1), 151–166, doi:10.1029/JA087iA01p00151.